ADVANCED MATERIALS

[21] J. Liu, A. G. Rinzler, H. Dai, J. H. Hafner, R. K. Bradley, P. J. Boul, A. Lu, T. Iverson, K. Shelimov, C. B. Huffman, F. Rodriguez-Macias, Y.-S. Shon, T. R. Lee, D. T. Colbert, R. E. Smalley, *Science* **1998**, *280*, 1253.
[22] A. G. Rinzler, J. Liu, H. Dai, P. Nikolaev, C. B. Huffman, F. J. Rodriguez-macias, P. J. Boul, A. H. Lu, D. Heymann, D. T. Colbert, R. S. Lee, J. E. Fischer, A. M. Rao, P. C. Eklund, R. E. Smalley, *Appl. Phys. A – Mater. Sci. Process.* **1998**, *67*, 29.
[23] G. M. Spinks, L. Liu, D. Zhou, G. G. Wallace, *Adv. Funct. Mater.* **2002**, *12*, 437.

Rectangular Porous ZnO–ZnS Nanocables and ZnS Nanotubes**

By *Xudong Wang*, *Puxian Gao*, *Jing Li*, *Christopher J. Summers*, and *Zhong Lin Wang**

ZnS, an important wide-bandgap semiconductor, is a photoluminescence material.[1] Due to its wide bandgap of 3.8 eV, doping of ZnS with elements such as Tb and Eu,[2] can produce a wide range of exciting optical properties. Quantum dots of core–shell structured CdSe/ZnS have been found to exhibit a lasing effect and can be used for fluoro-immunoassays, biological imaging, and biosensors.[3,4] Quantum confinement induced lasing has been observed in CdSe/ZnS.[5]

Semiconducting ZnO is one of the most important functional oxides for smart devices and optoelectronics. Recently, ultra-long nanobelt structures of ZnO, SnO_2, In_2O_3, CdO, Ga_2O_3, and PbO_2 have been synthesized by simply evaporating the desired commercial metal oxide powders at high temperatures.[6,7] The as-synthesized oxide nanobelts are pure, structurally uniform, single crystalline, and most of them are free from dislocations. They have a rectangular cross section with typical widths of 100–300 nm, width-to-thickness ratios of 5–10 nm, and lengths of up to a few millimeters. The nanobelts are an ideal system for fully understanding dimensionally confined transport phenomena in functional oxides and for building functional devices along individual nanobelts. Nanosize sensors and field-effect transistors based on individual nanobelts have been fabricated.[8,9]

Colloid based methods are likely the most popular techniques for synthesis of semiconductor quantum dots.[10,11] Various forms of ZnS nanostructures have been synthesized, including nanoparticles,[12,13] nanowires,[14,15] and nanosheets.[16] In this paper, using as-synthesized ZnO nanobelts as a template, nanostructured ZnS nanocables and nanotubes have been synthesized by chemical reaction. The structure of the ZnS has been analyzed and the corresponding photoluminescence properties have been measured. A small blue shift is observed for the ZnO–ZnS cable structures, suggesting a small quantum-confinement effect. The template-assisted method is demonstrated to be a unique technique for producing ZnS nanostructures with controlled morphology.

We first present the structural change of the ZnO nanobelt pre- and post-reaction with H_2S. Figure 1a shows a scanning electron microscope (SEM) image of the as-synthesized ZnO nanobelts, which are pure and structurally uniform. A transmission electron microscope (TEM) image of the nanobelts is given in Figure 2a, clearly showing its uniformity in shape. The ZnO nanobelts have two fast growth directions, [0001] and $[10\bar{1}0]$.[6] For the [0001] ZnO nanobelts, the top surfaces are $\pm(2\bar{1}\,\bar{1}0)$, and the side surfaces are $\pm(01\bar{1}0)$. The contrast observed on the nanobelts is due to bending induced strain, which is the so-called bending contour in electron diffraction.[17]

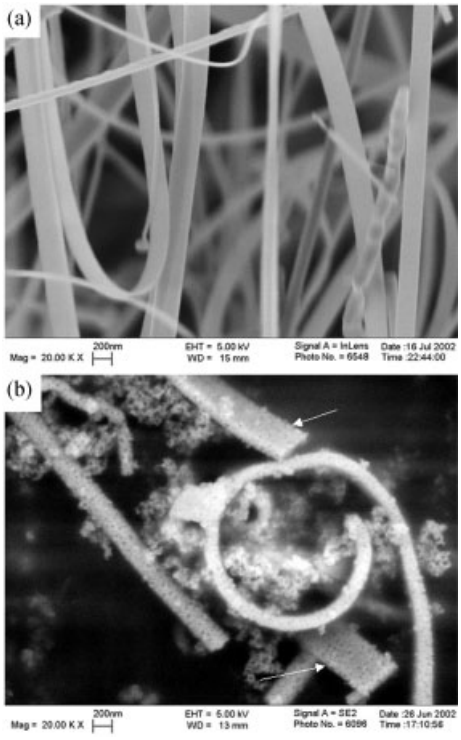

Fig. 1. SEM images of ZnO nanobelts a) pre- and b) post-reaction with H_2S, showing the change in surface morphology.

Based on the geometrical shape of the nanobelt template, we anticipate to receive ZnS nanostructures based on the reaction

$$ZnO + H_2S \longrightarrow ZnS + H_2O \quad (1)$$

Figure 1b shows a SEM image of the converted ZnS nanobelts. Indeed, besides some particle-shaped reaction products, nanobelts of ZnS have been formed, as indicated by arrowheads. But the nanobelts have porosity with pore sizes of ~30 nm. A rolled nanobelt is presented in the image, which is possibly produced by the surface tension introduced after the reaction; such a shape was rarely observed for the as-synthe-

[*] Prof. Z. L. Wang, X. Wang, P. Gao, Dr. J. Li, Prof. C. J. Summers
Center for Nanoscience and Nanotechnology, School of Materials Science and Engineering, Georgia Institute of Technology
Atlanta, GA 30332-0245 (USA)
E-mail: zhong.wang@mse.gatech.edu

[**] The authors are grateful for the financial support from the US NSF grant DMR-9733160 and the MURI program from ARO (DAAD19-01-1-0603), and thank the Georgia Tech Electron Microscopy Center for providing the research facility, and Dr. Chulsoo Yoon for his help in photoluminescence measurements.

  0935-9648/02/2312-1732 $ 17.50+.50/0

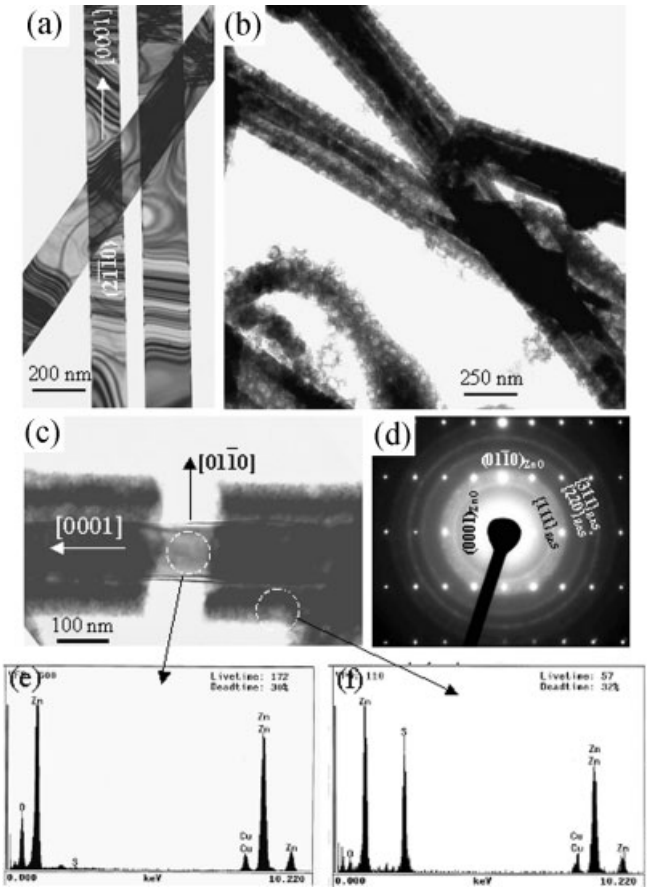

Fig. 2. TEM image of ZnO nanobelts a) pre- and b) post-reaction with H_2S, showing the formation of ZnO–ZnS nanocable structures. c) A ZnO–ZnS nanocable with a broken ZnS shell, and d) a corresponding electron-diffraction pattern recorded from the region, showing the presence of a single-crystalline ZnO core and the nanostructured ZnS shell. e,f) EDS spectra acquired from the regions indicated in (c), which prove the local chemical composition (the C and Cu lines come from the supporting films and copper grid used for TEM analysis, respectively).

sized ZnO nanobelts. TEM analysis shows that the converted ZnS nanobelts have two types of structural configurations: rectangular ZnO–ZnS nanocables and ZnS nanotubes.

Figure 2b shows a low-magnification TEM image of the ZnO–ZnS nanocables, with a single crystal ZnO as the core and the nanostructured ZnS as the shell. The interface between the shell and the core is fairly sharp and there appears to be no intermediate layer. A clearer picture of the structure is given in Figure 2c, which displays a composite nanocable with a broken ZnS surface layer. Electron diffraction recorded from the nanocable displays a spotted pattern that corresponds to the $[2\bar{1}\,\bar{1}0]$ zone axis of ZnO, and a set of ring diffraction patterns, which fits very well to zinc-blend structured ZnS. This is consistent with other studies that have shown that, for small particles, low-temperature synthesis leads to the zinc-blend structure,[16] while high-temperature synthesis results in the wurtzite structure.[14] Real-space distances measured from the rings also fit the expected inter-planar spacings for ZnS. Energy-dispersive X-ray spectroscopy (EDS) analysis shows that the core is mainly composed of Zn and O, and the shell is Zn and S, as shown in Figures 2e and 2f. Therefore, the core is a single crystalline ZnO and the shell is nanocrystalline ZnS.

The other type of structural configuration is ZnS nanotubes (Fig. 3a). The tubular shape of the ZnS nanostructured wall is apparent, and there is some porosity in the tube wall. The wall thickness can be as thick as ~100 nm (Fig. 3b) and as thin as 30 nm (Fig. 3c). Electron diffraction shows the random orientations of the ZnS nanocrystallites.

High-resolution TEM has been employed to study the ZnS nanocrystallites (Fig. 4). The ZnS layer is composed of small

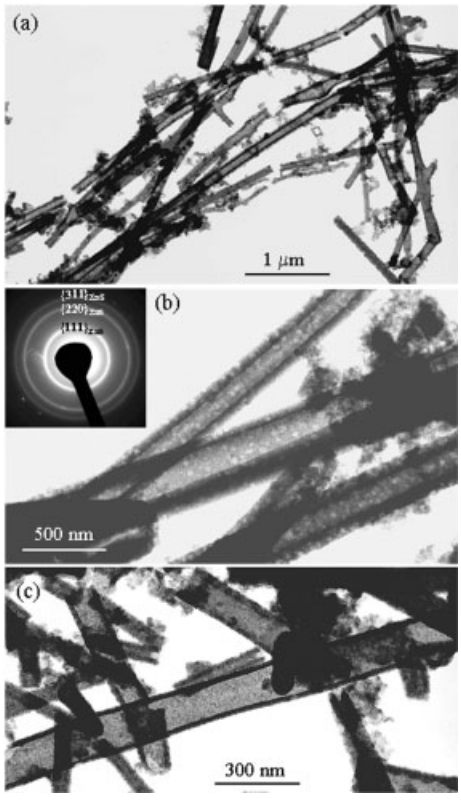

Fig. 3. a–c) Low-magnification and higher magnification TEM images of ZnS nanotubes. An electron-diffraction pattern recorded from the tubes is inserted, which can be indexed to be ZnS zinc blend structure.

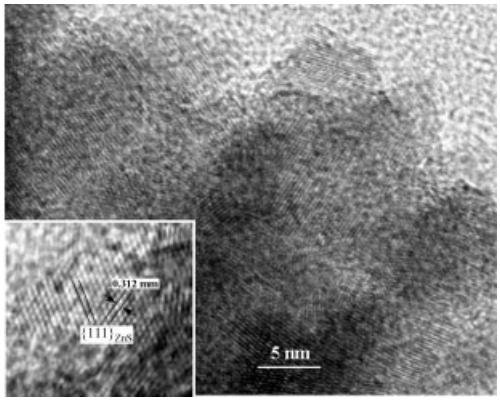

Fig. 4. High-resolution TEM image of ZnS nanocrystallites in the shell of a ZnO–ZnS nanocable, showing their grain size, crystallinity, and distribution.

  0935-9648/02/2312-1733 $ 17.50+.50/0

ADVANCED MATERIALS

size nanocrystals, whose average size is ~7 nm. The lattice symmetry can be seen through a [110] projected image given in the inset, which displays the two sets of {111} fringes and (002) fringes.

The conversion of ZnO nanobelts into ZnS nanocrystallite structured nanocables and nanotubes occurred in solution. The nanocable is formed by a direct reaction of H_2S with the surface layer of ZnO within the presence of water, by

$$ZnO + H_2O \longrightarrow Zn^{2+} + 2(OH)^- \quad (2)$$

$$H_2S \longrightarrow H^+ + (HS)^- \longrightarrow 2H^+ + S^{2-} \quad (3)$$

A combination of Equations 2 and 3, gives

$$ZnO + H_2O + H_2S \longrightarrow ZnS + 2H_2O \quad (4)$$

Due to the limited solubility of ZnO in water, the reaction is essentially a substitution reaction; thus, the nanocable still preserves the rectangular cross section. The pores in the structures are produced due to two factors. First, excess H_2O produced in the reaction may be present in the structure and form the pores. Second, from the structural point of view, ZnS has the zinc-blend structure (cubic) with $a = 0.54109$ nm, and ZnO has the wurtzite structure (hexagonal) with $a = 0.3249$ nm and $c = 0.52065$ nm; both of them are incompatible in structure. Thus, the substitution reaction is unlikely to produce single crystalline ZnS. The formation of nanocrystallites is expected, especially because the reaction took place at room temperature.

The formation of nanotubes is possible if the Zn^{2+} and $(OH)^-$ ions are mobile in the solution, so that they can diffuse through the porous ZnS wall and combine with the H^+ and S^{2-} ions in the solution, resulting in the formation of an empty tubular structure.

The photoluminescence (PL) property of the ZnO–ZnS nanostructures has been measured. A comparison of the PL spectra recorded from the as-synthesized ZnO nanobelts, the ZnO–ZnS nanocables and ZnS powders is given in Figure 5. The peak located at ~385 nm corresponds to the 3.2 eV bandgap transition of ZnO. A small blue shift of ~2 nm for the ZnO–ZnS nanocables is observed (see the inset) that is possibly due to the reduced size of the ZnO cores, especially in the thickness direction of the nanobelt. The peak located at 470 nm is contributed by ZnS and the broad peak at 550 nm is a resultant contribution from ZnO and ZnS.

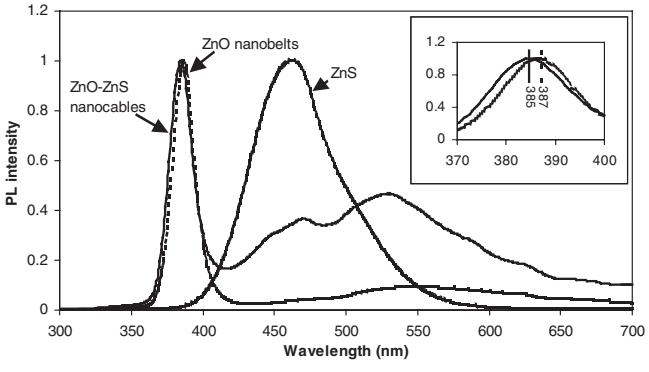

Fig. 5. Photoluminescence spectra acquired from the as-synthesized ZnO nanobelts, the standard ZnS sample, and the ZnO–ZnS nanocables. The inset is an enlargement of the peak around 385 nm, showing a ~2 nm blue shift for the ZnO–ZnS nanocables.

In summary, using ZnO nanobelts as a template, nanostructured ZnO–ZnS nanocables and ZnS nanotubes have been synthesized for the first time. These structures are made of ZnS nanocrystallites of ~7 nm and have a high percentage of pores. For the bandgap characteristic peak of 386 nm for ZnO, a small blue shift is observed in the photoluminescence spectrum from the ZnO–ZnS nanocables, possibly indicating a small quantum-confinement effect. The new ZnO–ZnS composite nanostructures may have useful applications for advanced luminescence materials. The method demonstrated here could be a general approach of fabricating nanobelt-based porous structures of compound semiconductors.

Experimental

The ZnO nanobelts were synthesized by a solid–vapor process reported in detail elsewhere [6]. Saturated H_2S (> 0.4 %) was obtained from Fisher Scientific and filtered before reaction. All of the other chemicals were purchased from Alfa Aesar and used as-received. The water used in all experiments had a resistivity higher than 18.2 MΩ cm. 50 mg of ZnO nanobelts was added into 3 mL of pure ethanol. After 10 min of the application of ultrasound, a well-dispersed ZnO nanobelts suspension was obtained, and then 30 mL of saturated H_2S water was added. The mixture was sealed and stored for 24 h at room temperature. The resulting nanobelts were cleaned through three cycles of centrifugation (3000 rpm for 15 min) and re-dispersion in 10 mL of water. Finally, the solution was dried in an isothermal oven at 90 °C (the synthesis temperature of a ZnO nanobelt is ~1350 °C).

Photoluminescence (PL) spectra were acquired by placing ZnO nanobelts on an Al_2O_3 substrate, and the data shown are the processed results that have the contribution from Al_2O_3 removed. PL measurements of ZnS–ZnO nanocables and the standard ZnS were made using powders of these materials. Photon excitation was stimulated using a Beamlok 2085-15 Ar-ion laser (275 nm) and the spectra were acquired using an Isa 270m spectrometer and photomultiplier tube (PMT).

Samples for transmission electron microscopy (TEM) were prepared by placing a droplet of the suspension of nanobelts onto a carbon-coated copper grid and allowing the solvent to evaporate. Scanning electron microscopy (SEM) measurements were performed using a LEO 1530 FEG SEM at 5 kV. TEM analysis was carried out using a Hitachi HF2000 microscope operated at 200 kV. Energy-dispersive X-ray spectroscopy (EDS) analysis was performed during TEM measurements.

Received: July 19, 2002

[1] For a review see: P. D. Rack, P. H. Holloway, *Mater. Sci. Eng. Res.* **1998**, *21*, 171.
[2] M. Ihara, T. Igarashi, T. Kusunoki, K. Ohno, *J. Electrochem. Soc.* **2002**, *149*, H72.
[3] P. T. Tran, E. R. Goldman, G. P. Anderson, J. M. Mauro, H. Mattoussi, *Phys. Status Solidi B* **2002**, *229*, 427.
[4] E. R. Goldman, E. D. Balighian, H. Mattoussi, M. K. Kuno, J. M. Mauro, P. T. Tran, G. P. Anderson, *J. Am. Chem. Soc.* **2002**, *124*, 6378.
[5] M. Kazes, D. Y. Lewis, Y. Ebenstein, T. Mokari, U. Banin, *Adv. Mater.* **2002**, *14*, 317.
[6] Z. W. Pan, Z. R. Dai, Z. L. Wang, *Science* **2001**, *291*, 1947.
[7] Z. W. Pan, Z. R. Dai, Z. L. Wang, *Appl. Phys. Lett.* **2001**, *80*, 309.
[8] E. Comini, G. Faglia, G. Sberveglieri, Z. W. Pan, Z. L. Wang, *Appl. Phys. Lett.* **2002**, *81*, 1869.
[9] M. S. Arnold, P. Avouris, Z. W. Pan, Z. L. Wang, *J. Phys. Chem. B*, in press.
[10] A. Henglein. *Chem. Rev.* **1989**, *89*, 1861.

  0935-9648/02/2312-1734 $ 17.50+.50/0

[11] A. P. Alivisatos, *Science* **1996**, *271*, 933.
[12] W. Z. Wang, I. Germanenko, M. S. El-Shall, *Chem. Mater.* **2002**, *14*, 3028.
[13] E. J. Donahue, A. Roxburgh, M. Yurchenko, *Mater. Res. Bull.* **1998**, *33*, 323.
[14] Y. W. Wang, L. D. Zhang, C. H. Liang, G. Z. Wang, X. S. Peng, *Chem. Phys. Lett.* **2002**, *357*, 314.
[15] X. C. Jiang, Y. Xie, J. Lu, L. Y. Zhu, W. He, Y. T. Qian, *Chem. Mater.* **2001**, *13*, 1213.
[16] S. H. Yu, M. Yoshimura, *Adv. Mater.* **2002**, *14*, 296.
[17] Z. L. Wang, Z. C. Kang, *Functional and Smart Materials–Structure Evolution and Structure Analysis*, Plenum, New York **1998**.

The Effect of a Mild Thermal Treatment on the Performance of Poly(3-alkylthiophene)/Fullerene Solar Cells**

By *Nadia Camaioni*,* *Giovanni Ridolfi*, *Giuseppe Casalbore-Miceli*, *Giorgia Possamai*, and *Michele Maggini*

The potential for using functionalized fullerenes as electron acceptors (A) in composite films with conjugated polymers has been highlighted by recent results showing that solar cells reaching power conversion efficiencies of up to 3.3 %, under AM1.5 standard test conditions, could be fabricated.[1,2] Upon photoexcitation, an ultrafast electron transfer takes place from the polymer (the electron-donor component, D) to the fullerene: the process is reversible, and metastable with a quantum yield close to 100 %.[3]

A key factor that influences the power conversion efficiency (η) of D/A solar cells is the charge carrier mobility, which is strongly related to the structural order of the donors and acceptors in the active layer. It is well-known that an enhanced degree of crystallinity can be induced in polythiophene films by thermal annealing,[4] or by treatment with chloroform vapor.[5] Parallel to this, a shift of the maximum absorption towards longer wavelengths is usually observed in the visible spectrum of the polymer.[5] In this connection, devices made of polythiophene with pendant fullerenes show an increase in their external quantum efficiency (EQE) upon treatment of the active layer with chloroform vapor.[6] An increase in EQE by a factor of about 1.6 has been also obtained by annealing a blend made of regioregular poly(3-hexylthiophene) and a perylene derivative at 80 °C for 1 h.[7]

A high EQE is a necessary condition for high photovoltaic efficiency, but not sufficient. In this paper, we report results that demonstrate how a mild thermal treatment of polythiophene/fullerene solar cells significantly enhances their power conversion efficiency.

Regioregular poly(3-hexylthiophene, PHT) and poly(3-octylthiophene, POT) were used as the donors, and a soluble fulleropyrrolidine (**1**, Fig. 1) was used as the acceptor.

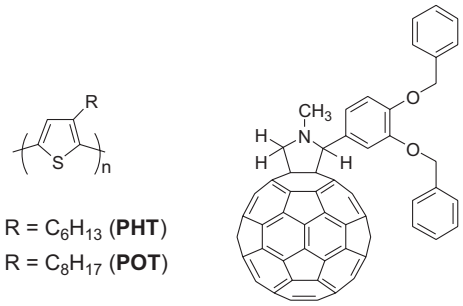

Fig. 1. Structure of the polythiophenes and fulleropyrrolidine used in this study. The latter was chosen because it is readily soluble in the solvent ($CHCl_3$) used for spin-coating depositions.

Cells with different D/A weight ratios (WR) were prepared and, in all the investigated cases, an impressive and permanent improvement in the device performance was obtained upon heating the devices, under dynamic vacuum, to a temperature as low as 55 °C for 30 min in the chamber used for the electrical characterization. The cells were illuminated through the top, semitransparent aluminum electrode (10–11 nm thick), because the frame of the characterization chamber does not allow irradiation through the indium tin oxide (ITO) electrode without breaking the vacuum. As a consequence of the high optical losses through the Al layer, the η values are rather poor. However, the significance of the results reported herein is in the relative variation of the cell performance. A dramatic increase in the short-circuit current (j_{sc}) was observed by raising the temperature of the cells to just a few degrees above room temperature. As an example, Figure 2 shows the variation of the principal photovoltaic param-

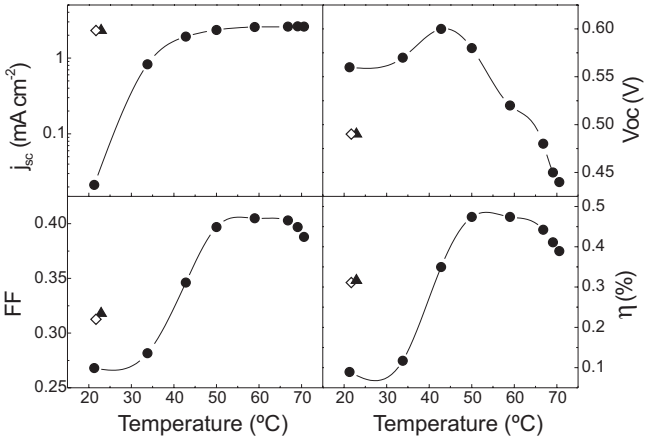

Fig. 2. Variation of the photovoltaic parameters during the first thermal process of a PHT/**1** cell (3:2 WR, full circles) and their values after cooling to room temperature (triangles), and after a successive temperature scan between 22 and 0 °C (diamonds). Linear temperature gradient at ca. 1 °C/min. P_{in}: 110 mW cm^{-2}. Transmittance of the Al layer: 14 % (at the maximum absorption wavelength of the active layer). The lines are drawn as a guide to the eye.

[*] Dr. N. Camaioni, Dr. G. Ridolfi, Dr. G. Casalbore-Miceli
Istituto CNR–ISOF
Via P. Gobetti 101, I-40129 Bologna (Italy)
E-mail: camaioni@frae.bo.cnr.it
Dr. G. Possamai, Prof. M. Maggini
Dipartimento di Chimica Organica, Università di Padova
Via Marzolo 1, I-35131 Padova (Italy)
E-mail: michele.maggini@unipd.it

[**] We thank Dr. R. Mendichi (ICM–CNR, Milano) for the molecular weight determination of the polythiophenes. This work was supported by CNR within the framework of the *Progetto Finalizzato Materiali Speciali per Tecnologie Avanzate II* and *legge 95/95*. MM thanks the MIUR (contract No. MM03198284) for financial support.

  0935-9648/02/2312-1735 $ 17.50+.50/0